INL/CON-07-12073
PREPRINT

Preliminary Study of Turbulent Flow in the Lower Plenum of a Gas-Cooled Reactor

NURETH-12

D. P. Guillen
H. M. McIlroy, Jr.

September 2007

The INL is a
U.S. Department of Energy
National Laboratory
operated by
Battelle Energy Alliance

PRELIMINARY STUDY OF TURBULENT FLOW IN THE LOWER PLENUM OF A GAS-COOLED REACTOR

D.P. Guillen and H.M. McIlroy, Jr.
Idaho National Laboratory
Idaho Falls, Idaho 83406
Donna.Guillen@inl.gov; Hugh.McIlroy@inl.gov

ABSTRACT

A preliminary study of the turbulent flow in a scaled model of a portion of the lower plenum of a gas-cooled advanced reactor concept has been conducted. The reactor is configured such that hot gases at various temperatures exit the coolant channels in the reactor core, where they empty into a lower plenum and mix together with a crossflow past vertical cylindrical support columns, then exit through an outlet duct. An accurate assessment of the flow behavior will be necessary prior to final design to ensure that material structural limits are not exceeded. In this work, an idealized model was created to mimic a region of the lower plenum for a simplified set of conditions that enabled the flow to be treated as an isothermal, incompressible fluid with constant properties. This is a first step towards assessing complex thermal fluid phenomena in advanced reactor designs. Once such flows can be computed with confidence, heated flows will be examined. Experimental data was obtained using three-dimensional Particle Image Velocimetry (PIV) to obtain non-intrusive flow measurements for an unheated geometry. Computational fluid dynamic (CFD) predictions of the flow were made using a commercial CFD code and compared to the experimental data. The work presented here is intended to be scoping in nature, since the purpose of this work is to identify improvements that can be made to subsequent computations and experiments. Rigorous validation of computational predictions will eventually be necessary for design and analysis of new reactor concepts, as well as for safety analysis and licensing calculations.

KEYWORDS
gas-cooled reactor, computational fluid dynamics, particle image velocimetry

1. INTRODUCTION

Advanced reactor designs incorporate inherent safety features not available in present day nuclear reactors. In the reactor concept investigated herein, helium coolant flows vertically downward through the core and enters the lower plenum through a series of jets into a cross flow. The radial variation of the core power density creates jets of differing temperatures. The hot gas jets exit into the plenum, then turn and flow horizontally past arrays of vertically-oriented cylindrical support posts to the outlet duct, where the gases are funneled to either a turbine or an intermediate heat exchanger for the production of electricity and/or hydrogen. Adequate mixing of the coolant flow is necessary to ensure

that material structural temperature limits are not exceeded in the lower plenum or power conversion machinery.

The objective of this study is to model a section of the lower plenum of an advanced reactor concept using a commercial computational fluid dynamics (CFD) code and compare the results to experimental data [1]. The lessons learned from this work should be applied towards future studies. A scaled model of a sub-region in the lower plenum was constructed and velocity field measurements were obtained using three-dimensional Particle Image Velocimetry (PIV). Analysis of the flow by [2] was performed for the simplified case of an unheated, constant property fluid. This analysis neglects buoyancy-driven flow effects and is considered representative of normal low-power operation These unheated MIR experiments provide data for the baseline case of negligible buoyancy and constant fluid properties, which are a first step to assess the fidelity of the CFD simulations. Once such flows can be computed with confidence, nonadiabatic flows will be examined.

2. EXPERIMENTS

Three-dimensional PIV data was obtained in the Matched-Index-of-Refraction (MIR) Facility at the Idaho National Laboratory (INL). The MIR uses an optical technique, PIV, to obtain non-intrusive flow measurements. The experiments were conducted to study the turbulent flow behavior and to produce data to compare to CFD predictions. The PIV system provides instantaneous and ensemble-averaged velocities at discrete points in the flow.

The model shown in Figure 1 mimics an infinite array of vertical cylindrical support posts arranged on an equilateral triangular pitch. A symmetrical arrangement of five cylindrical columns along the model centerline and ten half-cylinders along the two parallel side walls extend the full height of the model. The columns and inlet jets are 0.03175 m and 0.02210 m in diameter, respectively. The model measures 0.05398 m in width, 0.558 m in length, and 0.21750 m in height. The ratio of the spacing between the post centerlines, L, and the post diameter, D, is L/D=2.94. The relative scale of the model to the full-scale lower plenum section is 1:6.55 [3].

The experiments, although conducted at room temperature, can be directly scaled to the behavior in the prototypical system since at operational conditions the flow is momentum-dominated with negligible buoyancy and nearly constant fluid properties. Scaling studies have been performed to ensure that the flow test model with mineral oil flow under isothermal conditions duplicates the pertinent non-dimensional parameters in the lower plenum [2]. The model was constructed of quartz, an optically transparent material with the same index of refraction as the mineral oil used as the working fluid of the MIR system. Seeded mineral oil with a precisely controlled temperature of 23.3 ºC enters through four inlet ports above the model. The Reynolds number, based upon jet diameter and bulk flow velocity, is approximately 4300. Mineral oil from the main tunnel flows around the model at a velocity of 0.2 m/s, and mixes with the plenum flow at the model outlet.

The experiment is designed to simulate the flow in the central portion of the lower plenum, away from the outlet duct. The source of flow entering this region comes from jets exiting short coolant ducts at the corners of the hexagonal blocks, represented in the flow test model as a series of inlet jets located above the plenum. A solid wedge-shaped element at the upstream end simulates the hexagonal support block for the outer reflector and blocks cross flow from the main tunnel flow. The wedge partially blocks the inlet jet at the upstream end.

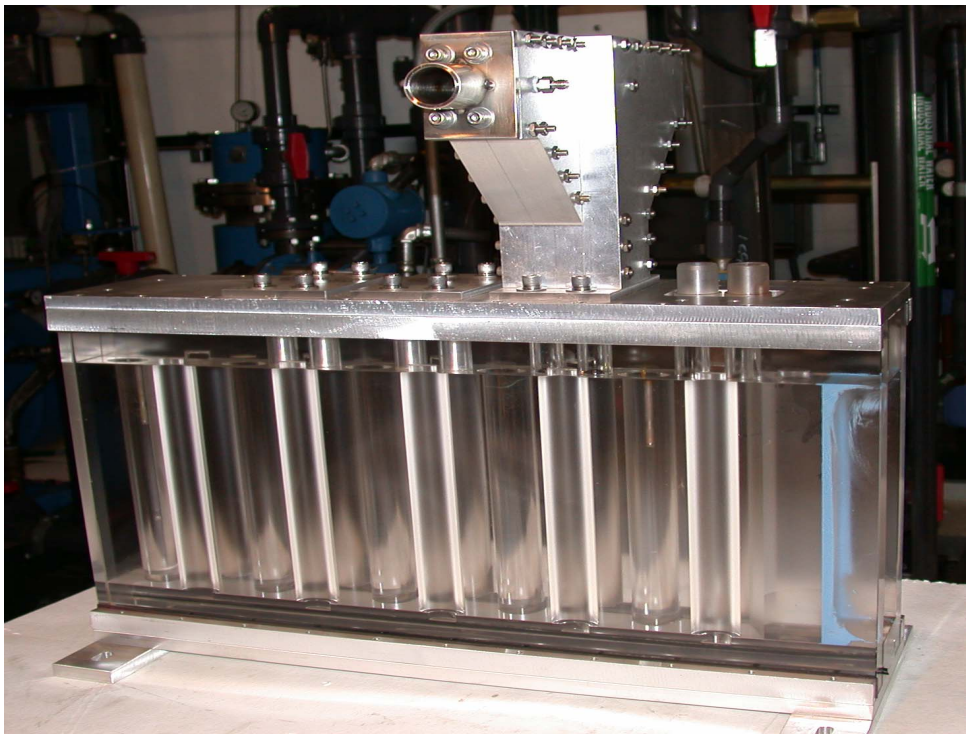

Figure 1 MIR flow test model.

3. COMPUTATIONS

A three-dimensional computational mesh was created to replicate the geometry and dimensions of the test model. The experimental conditions were modeled using the commercial CFD code FLUENT version 6.3. In this study, the segregated solver uses a point Gauss-Seidel technique and algebraic multigrid V-cycle acceleration. The control volume technique consists of integrating the governing equations for each control volume, yielding discrete equations that conserve each quantity on a control volume basis. FLUENT stores discrete values of the conserved quantity at the cell centers and uses an upwind technique for determining face values of the conserved quantity for the convective terms. A PREssure STaggering Option (PRESTO) scheme was used as the interpolation scheme for calculating cell-face pressures. The Pressure-Implicit with Splitting of Operators (PISO) scheme, which uses a combination of continuity and momentum equations to derive an equation for pressure, was used for pressure-velocity

coupling. The PISO algorithm performs both neighbor and skewness correction to decrease the number of iterations required for convergence of transient problems. The Monotone Upstream-Centered Schemes for Conservation Laws (MUSCL) scheme was used to interpolate the field variables (stored at cell centers) to the faces of the control volumes. This scheme produces a locally third-order convective discretization for unstructured meshes. The adaptive time-stepping feature in FLUENT invoked a time-step for the computations that varied between 0.01 and 0.02 seconds as the solution approached convergence.

FLUENT was used to solve the unsteady, Reynolds-averaged Navier-Stokes (RANS) equations for the turbulent flow present in the scaled model. RANS simulations treat the flow variables as having a time-averaged (mean) part and a turbulent part. This CFD application employs a turbulence model known for its robustness, economy and reasonable accuracy over a wide range of turbulent flows common in industry. The entire range of turbulence scales is modeled, and only mean flow features are resolved.

For the FLUENT study, the realizable k-ε (where k is turbulent kinetic energy [TKE] and ε is the TKE dissipation rate) turbulence modeling option with enhanced wall treatment was used. The enhanced wall treatment, a near-wall modeling method, combines a two-layer model with enhanced wall functions that are valid even in the wall buffer region ($3 < y+ < 10$). The wall functions were developed by smoothly blending the laminar (linear) and the turbulent (logarithmic) laws-of-the-wall. The realizable k-ε model is recommended over the standard k-ε model for problems where the flow features include strong streamline curvature and vortices [4]. The k-ε turbulence model solves for total TKE assuming turbulent viscosity is isotropic. However, the generation of TKE due to mean flow gradients may be different depending on which mean flow velocity gradients are being considered.

Systematic grid convergence tests are necessary to reduce numerical uncertainty by ensuring that the resolution of the computational mesh is adequate [5]. A difficulty associated with attempting to perform a grid convergence study using unstructured grids is the generation of a suitable succession of grids that retain the appropriate wall y+ value. To determine how fine a grid resolution was needed, a grid refinement study was performed using three grids of successively varying mesh refinement. The “medium,” “fine,” and “super-fine” meshes shown in Figures 2a-c were generated using the Gridgen software package [6]. The “medium” mesh was comprised of 225,243 cells, the “fine” mesh was comprised of 839,759 cells, and the “super-fine” grid was comprised of 1,265,292 cells. The unstructured grids were adapted to a polyhedral grid, which improved the speed of the calculations and yielded similar results. The “medium” polyhedral mesh was comprised of 328,816 cells, the “fine” polyhedral mesh was comprised of 689,857 cells, and the “super-fine” polyhedral mesh was comprised of 1,050,320 cells. Figure 2 shows the manner in which the adaptation procedure clustered the grid nodes in regions adjacent to solid walls (i.e., boundary layers).

It is a challenge for the CFD model to contain a fine enough mesh to fully simulate the physical conditions in the experimental model, including the boundary layers on the

walls. The goal of this study was to determine whether a k-ε turbulence model and "super-fine" grid resolution can adequately capture the flow phenomena.

The average global cell size, h, is defined as [7]

$$h = \left[\frac{1}{N} \sum_{i=1}^{N} (\Delta V_i) \right]^{\frac{1}{3}} \qquad (1)$$

Table 1 lists the average global cell size calculated using Equation 1 for the nine grids generated for this study. The volume of the fluid domain is 0.0075 m^3. The refinement factor (i.e., $h_{original}/h_{refined}$) ranges from 1.2 to 1.6.

Table 1. Average global cell size for the computational meshes generated for this study.

Level of refinement	Average global cell size, h (m)	
	FLUENT grids	
	unstructured	polyhedral
"medium"	0.0032	0.0028
"fine"	0.0021	0.0022
"super-fine"	0.0018	0.0019

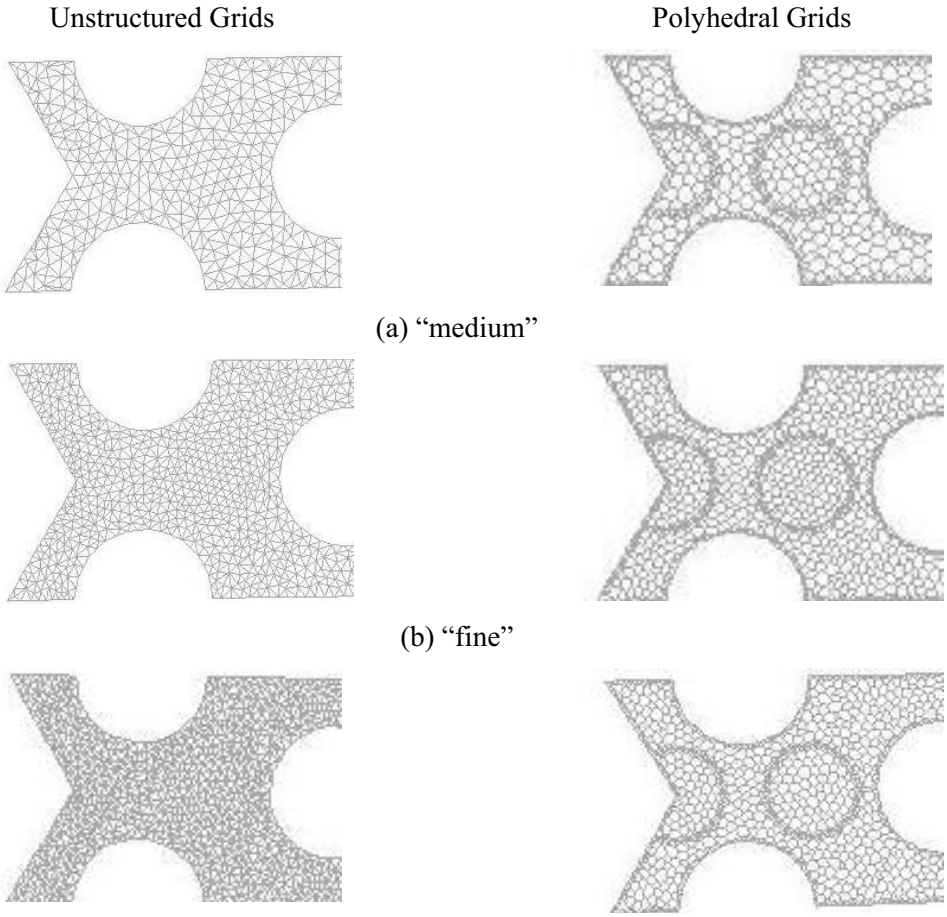

Figure 2 Detail sections of meshes created for grid independence study using FLUENT.

Simulations were run using the “fine” unstructured mesh and the results at specified points within the flow were compared to results obtained on the “super-fine” unstructured mesh. For the “super-fine” unstructured mesh, the values of wall y^+ varied between 0.108 and 13.66, with an average value of approximately 4. For the “super-fine” polyhedral

mesh, the values of wall y^+ varied between 0.009 and 11.33, with an average value of approximately 3.

Wall boundary conditions were specified for the surfaces of the circular cylinders and half cylinders; the channel sides, top, and bottom; the hexagonal wedge; and the sides of the inlet jets. A no-slip condition was enforced at the walls. To enable specification of the flow outlet as a constant pressure outlet, the model was extended 0.3062 m beyond the physical model outlet (located at x=0.5588 m). The frictional pressure drop caused by this artificial extension is less than 8 Pa. The backflow TKE was set to 0.04 m^2/s^2, and the turbulent dissipation rate, ε, was set to 1.0 m^2/s^3. The initial conditions specified were the x-, y-, and z- components of velocity and the static gage pressure set to zero (i.e., $V_x = V_y = V_z = P = 0$) . The working fluid in the MIR facility is mineral oil with a density of 831 kg/m^3 and a dynamic viscosity of 0.0118 kg/m·s.

Due to height restrictions in the laboratory, an elbow attached to the inlet flow conditioning block is located less than 6 inlet diameters upstream of the jet outlet into the plenum. The inlet manifold incorporates a 0.02057 m long honeycomb flow straightener, as well as two mesh screens for turbulence generation. Velocity data obtained within the jets at a location approximately 0.010 m above the plenum indicate that the flow is not fully developed, as would be expected since there is insufficient pipe length to produce fully developed flow. Also, inlet jet #1 is partially blocked by the hexagonal wedge and this flow obstruction disturbs the flow as it exits the inlet pipe.

Unfortunately, the interface between the jet outlet and the plenum was obscured due to the model construction and data could not be acquired at that location. Computations were initially run using the experimentally obtained inlet velocity profiles at a location approximately 0.01 m above the interface. However, it was found that, in this case, the PIV data point density and resulting limited number of velocity profiles were too coarse to adequately predict the mass flow rate. As a result, integration of the measured velocity profiles under predicts the mass flow rate in the jets by 20 to 40%. This necessitated the application of a mass flow rate boundary condition for the CFD model, rather than the use of velocity profiles at the inlet, to ensure conservation of mass. The mass flow rate boundary condition applied at the 4 inlet jets produced a uniform velocity across the inlet jet. For jet #1, the mass flow rate was set to 0.5898 kg/s and for jets #2, #3, and #4 the mass flow rate was set to 0.8782 kg/s. A similar dilemma was encountered when examining the measured turbulent kinetic energy profiles. They were found to be too coarse and irregular. An average TKE value of 0.04 m^2/s^2 based upon the measurements was used at the inlets. In reality, the distribution of turbulence will be complex and vary across the inlet jets. The rate of turbulence dissipation estimated at 1.0 m^2/s^3 based upon the following equation [8]

$$\varepsilon = c_\mu \frac{k^2}{\nu_t} \tag{2}$$

where c_μ is equal to 0.09 and ν_t is the turbulent viscosity. These parameters were applied at a location approximately 0.01 m above the jet/plenum interface to avoid having to modify the existing grid.

Residuals of mass, momentum, TKE, and ε were monitored to determine iterative convergence. In FLUENT, these residuals are normalized values. The Unsteady RANS (URANS) solution was allowed to iterate until the residuals reached $1x10^{-6}$ for mass and momentum and $1x10^{-5}$ for TKE and ε. These convergence tolerances were based on the research performed by Johnson [3]. The solution converged at each time step. The net difference in computed mass flux through the inlets and outlet is $1x10^{-7}$.

4. RESULTS AND DISCUSSION

Experiments conducted at Utah State University (USU) [9] were conducted to aid in characterizing the flow regimes in an array of staggered vertical cylinders in a confined channel. A cylinder array was designed to mimic the lower plenum design and match the primary geometric dimensionless parameters of the MIR flow test model. The dimensionless cylinder pitch, P/D, equals 1.7, where P is the distance between adjacent cylinders and D is the cylinder diameter. The spanwise height to cylinder diameter ratio, H/D, equals 6.9. The USU model does not have a hexagonal wedge blocking the flow at the upstream end because the inlet is located there. Air enters through the inlet at a uniform x-velocity and flows across vertically-oriented cylinders and half-cylinders in a confined channel. The instantaneous velocity field across a centerline cylinder was measured using PIV and the resulting observations used to categorize the flow behavior into identifiable regimes [9]. For Reynolds numbers between 400 and 510, unsteady laminar flow is present with unstable separated shear layers in the wake region behind the centerline cylinders. For Reynolds numbers between 600 and 1900, the flow is mixed partially-turbulent with turbulent flow present in expanding regions (where there are adverse pressure gradients) and laminar flow present in converging (accelerating) regions. For Reynolds numbers between 1900 and 7000, the flow exhibits mixed turbulent flow behavior wherein the flow outside the boundary layer is turbulent and the boundary layer on the cylinder remains laminar. Above a Reynolds number of 8000, the flow is fully turbulent. The test section Reynolds number is based upon the post diameter and the bulk velocity at the minimum area.

For the INL MIR configuration, the maximum computed time-averaged x-velocity (Vx=1.61 m/s) is located at the bottom of the plenum, just upstream of the hexagonal wedge. The post Reynolds number at this location is 3600. The measurements obtained by the INL MIR system (for a jet Reynolds number of 4300) indicate a maximum post Reynolds number of 4450. Based upon the USU flow regime classification, the flow is expected to be turbulent outside and laminar inside the boundary layer on the posts [9]. High frequency turbulent fluctuations will be superimposed on the nonstationary flow [3].

The inlet for the USU flow configuration is different than the INL MIR model, where the flow enters the plenum through inlets located at the top of the model. The inlet

configuration causes the flow to be highly three-dimensional for the INL MIR experiments. The downward flow from the inlets mixes with the fluid in the plenum causing the velocity to vary significantly in the y-direction, an effect that is pronounced near the inlet jets and diminishes as the flow travels downstream until it is homogeneous at the computational outlet boundary. A wake forms on the downstream side of each cylindrical support post with separation angles dependent upon flow speed (i.e., vertical location along the post). Figure 3 shows the variation in computed and measured x-velocity as a function of y-coordinate at spanwise centerline (z=0.0 m) for four x-locations (0.12022 m, 0.16850 m, 0.19807 m, and 0.26729 m). Figure 4 shows the locations of these planes relative to the model origin. The four inlet jets are depicted by the red open circles, with the jets numbered from 1 to 4 from right to left. Qualitative agreement between the experimental data is good, except for the data plane that bisects inlet jet #2. This can be attributed to the application of a mass flow rate boundary condition at the inlet jets, rather than using the actual turbulent velocity profile.

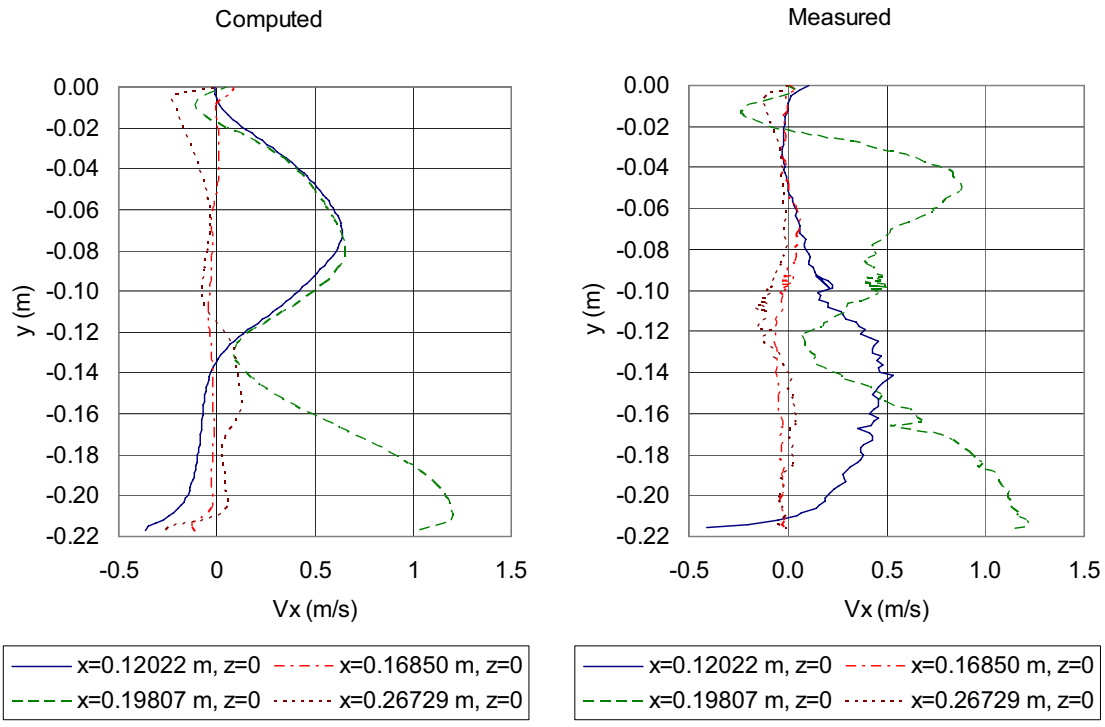

Figure 3 Variation of x-velocity as a function of y-location in plenum.

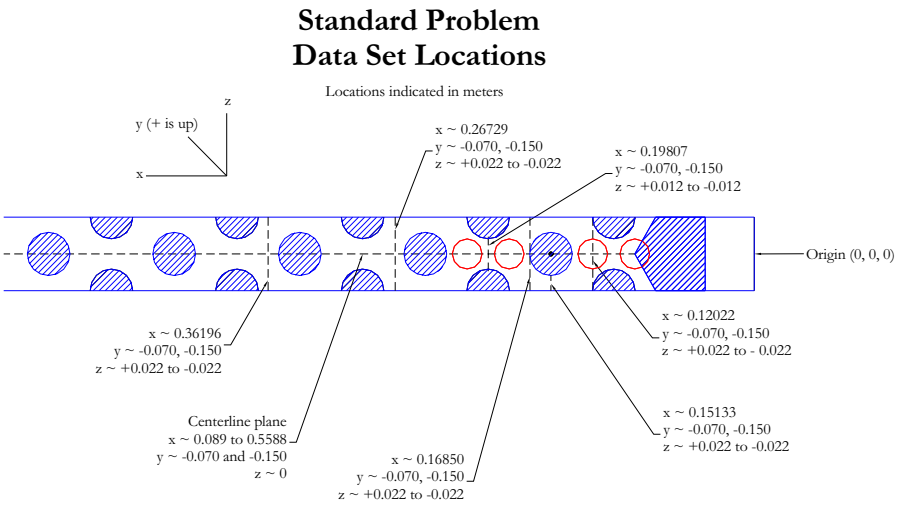

Figure 4 Data planes relative to model axis origin for data analysis.

The frequency of the vortices shed from the cylindrical support posts is approximated by:

$$w_v = \frac{V_x St}{d} \tag{3}$$

Vortex shedding occurs for $10^2 < Re_d < 10^7$, where Re_d is the post Reynolds number and the Strouhal number, St, remains approximately constant (≈0.2) over this range of Reynolds numbers [10]. Using the maximum computed x-direction flow velocity, Vx, the maximum vortex shedding frequency, w_v, is around 10 Hz. To capture the time progression of vortices shed from the cylinder, at least 20 data points per period should be acquired. This dictates a system response of at least 200 Hz for the data acquisition system.

Figure 5 shows a snapshot of flow in the lower plenum model with all four jets operating (McIlroy, et al., 2006). For visualization purposes, air is injected into the flow of the rightmost jet. Air was not injected into all four jets because the resulting mass of air bubbles made visualization of the flow structure impossible. The bubble-laden mineral oil flows downward into the plenum and exits through the outlet on the left. Areas of flow stagnation/recirculation, as well as those with enhanced mixing, are identified. The figure shows a complicated three-dimensional flow, with four large structures. The first structure is the vortex in the bottom right corner of the model where the bottom surface of lower plenum meets the outer reflector wall. The second structure is a mixing region in the vicinity of the first centerline support post in the bottom half of the model. The third structure is a second large vertical vortex downstream of the leftmost jet in the upper third of the model, and the fourth structure is the contour of the outlet flow as it passes beneath the third structure (large vortex) and expands vertically upward to cover the

entire exit area. These same structures can also be seen in the computational results by examining the time-averaged x-velocity shown in Figure 6. Qualitative agreement is good, but there are quantitative differences between the computed and measured results. For example, the experimental data indicate regions of negative x-velocity (Vx=-0.44 m/s) just beneath jet #1, in the corner region between the half post and model reflector. The computed solutions show reverse flow with a higher magnitude (i.e., Vx=-0.57 m/s). When the flow enters the plenum from jet #1, it has to negotiate the obstruction caused by the presence of the hexagonal wedge partially blocking the inlet. This effect was not modeled.

Since the PIV post-processing operation calculates ensemble-averaged flow quantities from the number of valid vectors identified in the instantaneous flow-field images, the CFD predictions were similarly averaged to enable a meaningful comparison with the data. Streamwise and spanwise slices located at approximately $^{1}\!/_{3}$ and $^{2}\!/_{3}$ the depth of the model ($y = -0.07$ m and $y = -0.15$ m) were selected to compare the computed and experimentally measured mean velocity and turbulence quantities.

In FLUENT, mean statistics are collected only in interior cells and not on wall surfaces. Therefore, the plots show velocities in cells adjacent to the wall. Additionally, the velocity field measurements in this PIV data set do not adequately resolve the near-wall velocity gradients because the spatial resolution used to interrogate the raw images were designed to investigate major flow phenomena and to characterize turbulence. Consequently the relatively large interrogation windows that were used could not accurately resolve velocity gradients inside the boundary layers. Due to this phenomenon, the measured velocity profiles at the inlet jets could not be used as a boundary condition.

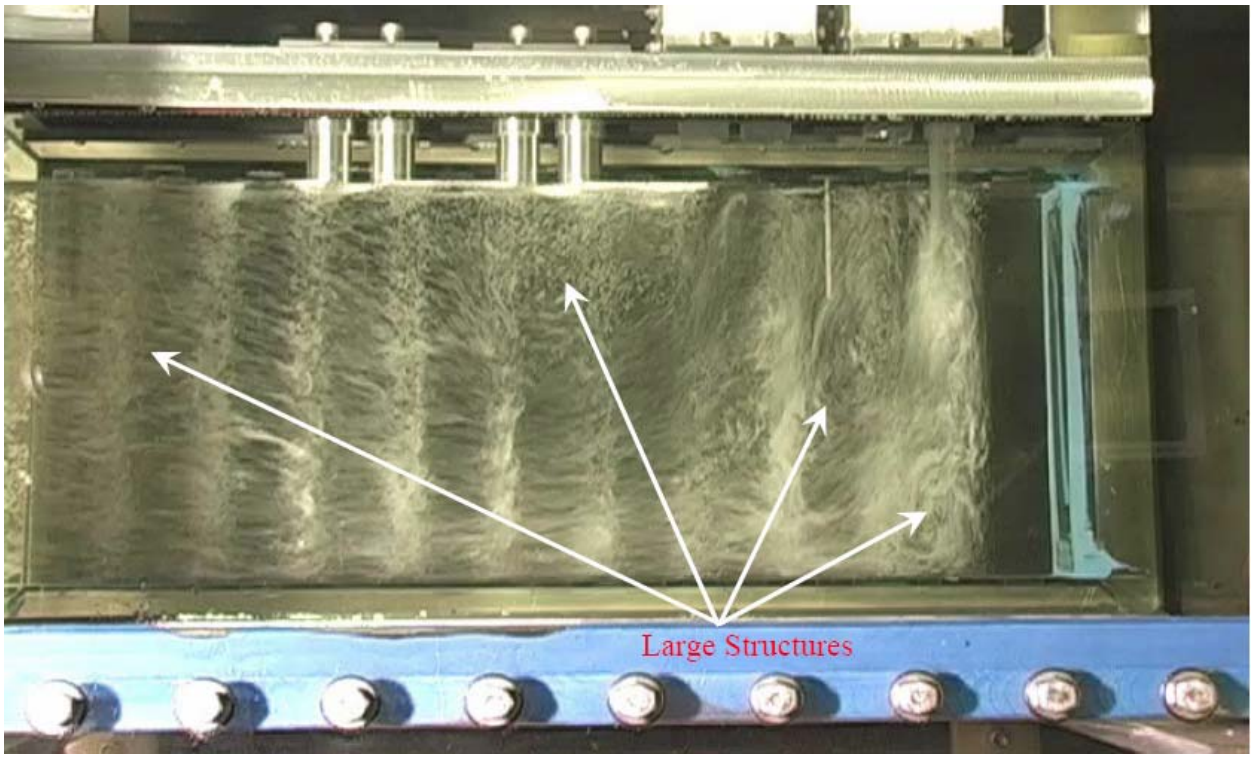

Figure 5 Flow visualization of four jets operating at jet Reynolds number of 4300.

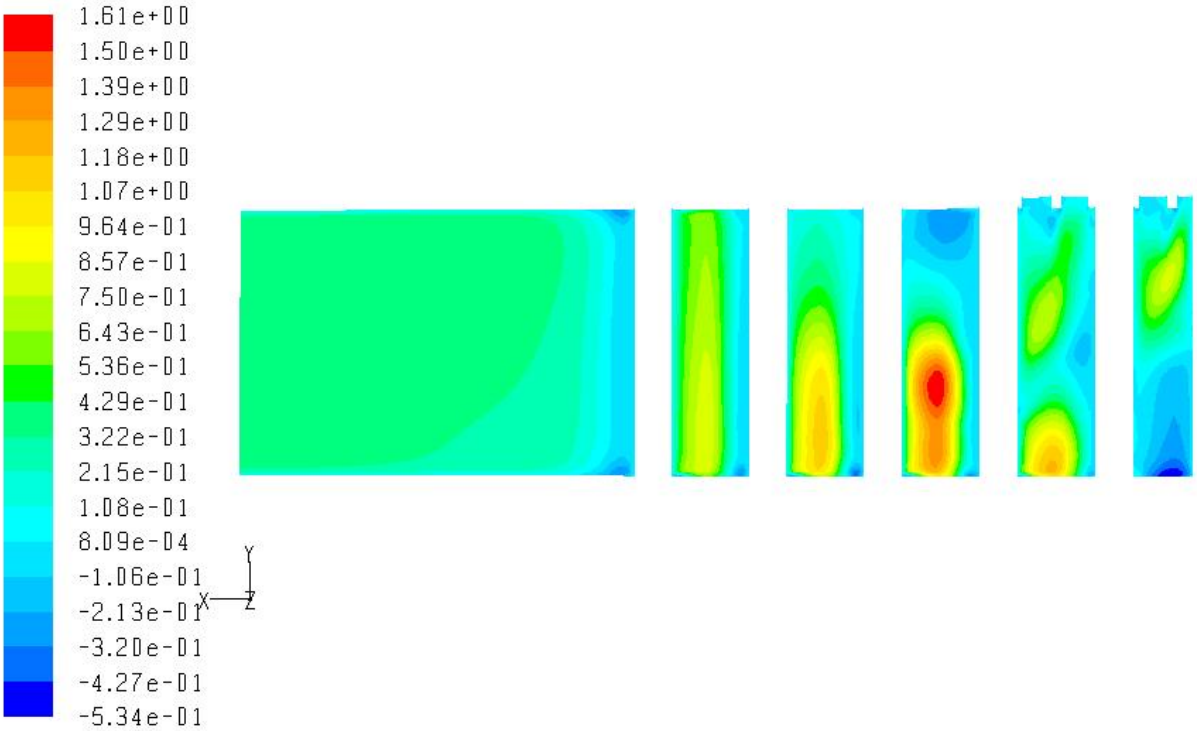

Figure 6 Computationally-predicted recirculation zones.

Figure 7 compares computed and measured velocities along the model centerline (z=0 m) at y-locations: −0.07 m and −0.15 m. The locations of the support posts are indicated by shaded gray bars. Experimental data is not available beyond the x=0.46 m location, because the test section supports blocked the camera views.

Figures 8 through 11 compare the computationally predicted velocities to experimental data at the following x-locations: 0.12022 m, 0.16850 m, 0.19807 m, and 0.26729 m, and y-locations: −0.07 m and −0.15 m. The largest values of velocity magnitude occur in the region below inlet jet #2 The computed long time-averaged velocity magnitudes in the region near the inlet jets differ from the measured values due to the boundary condition applied at the inlet jets. Downstream from the inlet jets, better agreement between the computed and measured values is seen.

Legend for Figures 7 to 12.

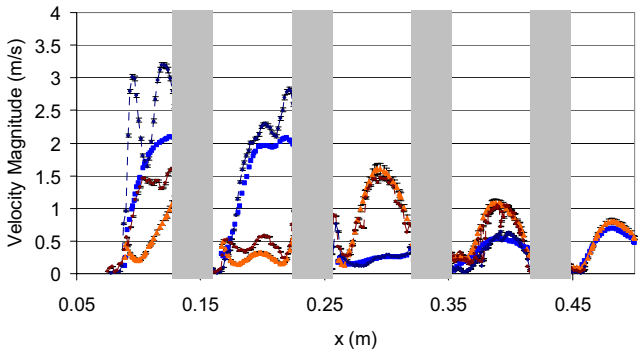

Figure 7 Velocities along the model centerline (z=0 m).

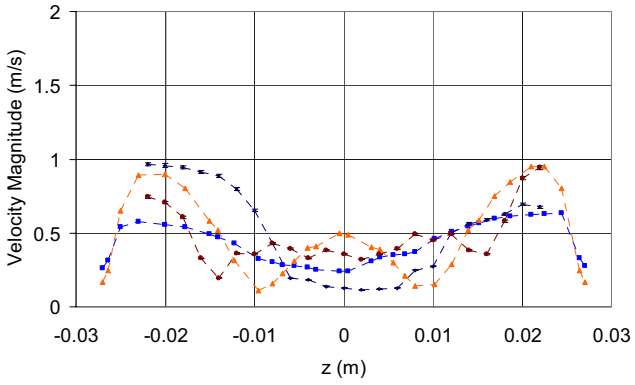

Figure 9 Velocities on a spanwise slice at x=0.16850 m.

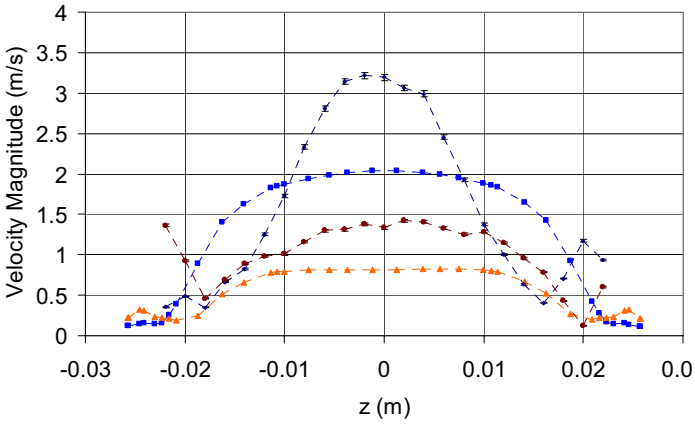

Figure 8 Velocities on a spanwise slice at x=0.12022 m.

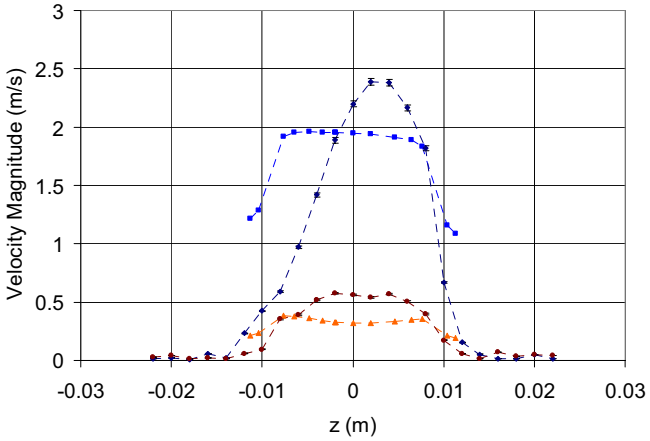

Figure 10 Velocities on a spanwise slice at x=0.19807 m.

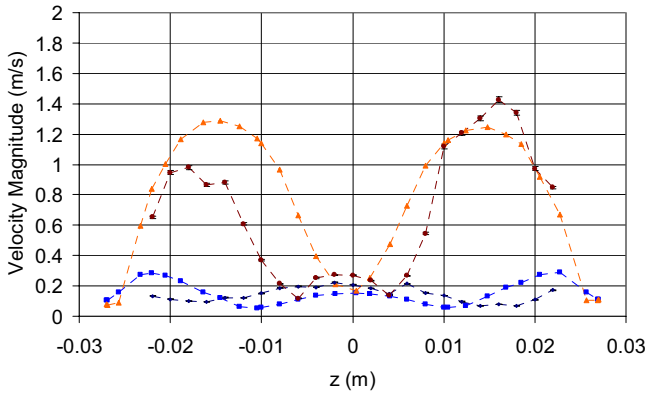

Figure 11 Velocities on a spanwise slice at x=0.26729 m.

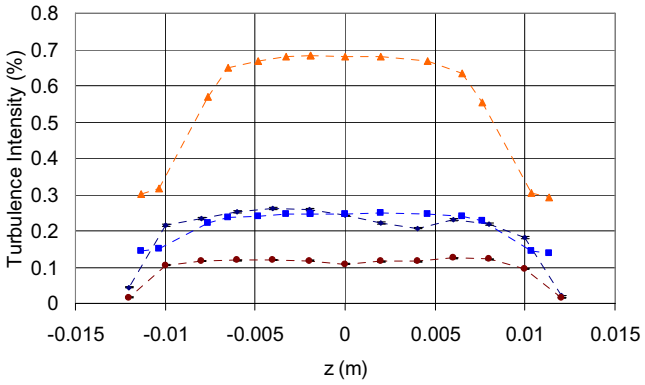

Figure 12 Turbulence intensity at x=0.19807 m.

Figure 12 compares the computed and measured turbulence intensity at x=0.19807 m and y=-0.07 m and y=-0.15 m. The values for turbulence intensity are normalized by the maximum velocity magnitude in that data slice. Agreement between computational results and the experimental data is better for the data slice located at the top $^{1}/_{3}$ of the plenum, than that at the lower $^{2}/_{3}$ of the plenum. The computed turbulence intensity reaches 68% in the lower region of the plenum, approximately 56% higher than the measured results indicate. This is attributed to the lack of suitable input data to define the turbulence at the inlet.

FLUENT converged more readily with the polyhedral grid than with the unstructured grid. The results presented in this paper were obtained using the "super-fine" polyhedral grid. Results obtained using the polyhedral grid more closely matched the experimental data than the results obtained using the unstructured grid, although the agreement was still far from optimal. Since the inlet boundary condition was not matched exactly, differences between the computed and measured results are expected. However, the large percentage difference in the computed mean velocity between the grids used in this study indicates that additional grid studies are needed. For future studies, computations should be performed on an even more refined grid until the results do not change between subsequent grids. In this study, the computational grids became unwieldy and the solutions required long execution times when the number of grid points was increased beyond that of the "super-fine" grid. The cost of sufficient FLUENT licenses to permit the use of massively parallel simulations on our high performance computing enclave was prohibitive.

5. SUMMARY AND CONCLUSIONS

Three-dimensional CFD predictions of flow through a complex geometry representing the lower plenum of an advanced reactor have been performed and compared with laboratory measurements obtained for a scaled model. The major trends seen in the experimental data are captured by the CFD results. The computed versus experimental results are in general agreement, but the quantitative agreement could be improved. Again, it is stressed that the purpose of this work is to better define improvements that can be made to the next set of computations and experiments. Better agreement between the computed and measured results could be achieved by modifying both the computational model and the laboratory setup. Discrepancies can be attributed to features of the current experimental setup and computational model. We recommend that the following areas be pursued in future studies:

- Model Design - Inlet Region. The obstruction created by the presence of the hexagonal wedge blocks the flow as it exits jet #1 and disturbs the velocity profile. Removal of this obstruction at the inlet would reduce flow complexity at the inlet. More data is necessary to better describe the inlet velocity profile.

- Model Design - Outlet Region. The last support post was located close to the model exit, creating a wake behind the post at that location. To achieve a constant pressure boundary at the model outlet, it was necessary to extend the computational model 0.3062 beyond the end of the flow test model. No experimental data were available at the exit plane of the flow test model, since the line-of-sight from the PIV system was blocked at this location. The main tunnel flow that was used primarily for index-matching temperature control, surrounds the exterior of the model and mixes with the flow exiting the model, whereas the computational model does not incorporate this mixing at the outlet plane. The mixing of flow at the model outlet with the main tunnel flow should be modeled.

- Data Acquisition – Time Resolution. The time-averaging procedure used by the computational code averages the results obtained at every time-step (approximately 0.01 sec), whereas the experimental setup averages the data measured at much larger time intervals (0.1 sec). To obtain sufficient data points to capture the flow unsteadiness, the data acquisition system should have the ability to capture data with sufficient resolution (i.e., >200 Hz). A high-speed PIV system could provide this data.

- Data Acquisition – Spatial Resolution. Due to the fact that the PIV method employed here is not accurate near the jet walls, the data in this region was missing. The profiles were also very coarse – in some locations there were only 8 data points representing the velocity profile at a given location across the jet. Thus, the velocity profiles, when integrated under-predicted the mass flow rate. To conserve mass in the plenum, a mass flow rate boundary condition was used, which employed a constant velocity across the inlet jet. Future studies should provide for the acquisition of adequate velocity and turbulent kinetic energy inlet profiles for use as boundary conditions to the computations. Consider using a different approach to obtain data at the inlet jets. Perhaps complementing PIV with laser Doppler velocimetry (LDV) could provide velocity data that, when integrated, yields the correct mass flow rates. LDV can resolve velocities in the proximity of the wall to about $y+<1$, which is more precise than PIV but much more time-intensive. The uncertainty in PIV is about 0.3 pixels. LDV uses much smaller control volumes.

- Data Acquisition – Additional Data. Currently, no pressure data is available. The experimental apparatus should be instrumented with pressure taps to enable comparison of computed versus measured pressure data.

- Turbulence Modeling. To accurately capture and represent turbulent mixing is a considerable experimental, theoretical and computational challenge [11]. Research by von Lavante and Laurien [12] shows that the k-ε turbulence model performs poorly for flows with strong streamline curvature, since the generation and dissipation of turbulence is anisotropic for these flows. For their application, two-equation turbulence models were found to be too dissipative and as a consequence rapidly dissipate the vorticity present in mixing regions. They found that

the Reynolds Stress Model (RSM) performs significantly better than the k-ε model when strong recirculation zones and eddies are present. For the lower plenum flow, the use of the RSM should be explored and the results compared with those obtained using the k-ε turbulence model.

- Grid Studies. Additional grid refinement using structured meshes should be performed until the solution is grid independent. The grid should be systematically refined until the solution does not change between refined grids. This necessitates using grids with more than 1.3×10^6 grid points, which will be very computer-intensive and not easily handled by the average industrial user. Because of this, it may be necessary to examine smaller regions in more detail rather than attempting to resolve flow details in a large region of the plenum.

The preliminary computations presented in this paper provide valuable information that can be used to guide further studies. Using computations to design the experiments is an approach that would facilitate code validation by conducting experiments that can be readily modeled and focusing resources on areas of complexity. The flow modeled herein is just one step towards obtaining a better understanding of the complex flow in the lower plenum of an advanced reactor. Wall effects on mixing in a confined channel are likely to cause significant differences between the actual lower plenum flow and that of the flow test model. The incorporation of thermal effects will also have a significant impact on the flow in this region. These effects must be accurately described in order to produce the necessary data for licensing and safety analysis of these advanced concept reactors.

ACKNOWLEDGMENTS

This manuscript has been authored by Battelle Energy Alliance, LLC under Contract No. DE-AC07-05ID14517 with the U.S. Department of Energy. References herein to any specific commercial product, process, or service by trade name, trademark, manufacturer, or otherwise, does not necessarily constitute or imply its endorsement, recommendation, or favoring by the U.S. Government, any agency thereof, or any company affiliated with Idaho National Laboratory.

REFERENCES

1. Schultz, R.R., et al., *Specifying Standard Problems for Validating Advanced Reactor Computational Fluid Dynamics Analysis Tools.* American Nuclear Society Transactions, 2006. 95: p. 836-837.
2. Condie, K.G., McCreery, G. E., McIlroy, H. M. Jr., and McEligot, D. M., *Development of an Experiment for Measuring Flow Phenomena Occurring in a Lower Plenum for VHTR CFD Assessment*. 2005, Idaho National Laboratory.
3. Johnson, R.W., *Modeling Strategies for Unsteady Turbulent Flows in the Lower Plenum of the VHTR*, in *CFD4NRS Workshop on Benchmarking of CFD Codes for Application to Nuclear Reactor Safety*. 2006: Garching, Munich, Germany.
4. *FLUENT*. 2007, FLUENT Inc.: Lebanon, NH, 03766.
5. Roache, P.J., *Verification and Validation in Computational Science and Engineering*. 1998: Hermosa Publishers.
6. *Gridgen*. 2006, Pointwise, Inc.: Forth Worth, TX.

7. Celik, I.B., *Procedure for Estimation and Reporting of Discretization Error in CFD Applications*, *Mechanical and Aerospace Engineering Department, West Virginia University*. 2006.
8. Celik, I.B., *Overview of Turbulence Modeling for Industrial Applications*, *Mechanical and Aerospace Engineering Department, West Virginia University*. 2006.
9. Smith, B.L., Stepan, J. J., and McEligot, D. M. *Velocity and Pressure Measurements along a Row of Confined Cylinders*. in *2006 ASME Fluids Engineering Summer Conference*. 2006. Miami, FL: Proceedings of ASME-FED 2006.
10. White, F.M., *Fluid Mechanics*. 5 ed. 2003: McGraw Hill. 312-313.
11. Dimotakis, P.E., *Turbulent Mixing.* Annual Review of Fluid Mechanics, 2005. 37: p. 329-356.
12. von Lavante, D., and Laurien, E. *Comparison of Turbulence Models for the Simulation of Hot Gas Mixing in the Lower Plenum of Pebble-Bed Type High-Temperature Reactors*. in *12th International Topical Meeting on Nuclear Reactor Thermal Hydraulics (NURETH-12)*. 2007. Pittsburgh, PA.